Interoperability of GNSSs for Position, Velocity and Timing

Alessandro Caporali[a], Joaquin Zurutuza[a]

[a] *University of Padova (Department of Geosciences), Via Giovanni Gradenigo, 6, 35131 Padova PD, Italy*

Abstract

Positioning by simultaneous tracking of multiple GNSSs requires that all the elements contributing to interoperability are properly calibrated. For example, the receiver time scale needs to be aligned to the timescales kept by the different GNSSs. Receiver-specific biases, need to be calibrated and the reference frame used in the representation of the orbits must be unique for all the involved GNSSs. In this paper we analyse multiGNSS data (GPS, Glonass, Galileo, BeiDou, QZSS, NAVIC, GAGAN and MSAS) of 19 stations of the worldwide GRC-MS (Galileo Reference Center - Member States) network, for the year 2020. We solve at each epoch for position, clock (one offset per constellation) and Tropospheric Zenith Delay. The time scales of Glonass, Galileo, QZSS, SBAS and NAVIC are shown to be very closely aligned to GPS, with constant offsets depending on receiver type. The offset of the BeiDou time scale to GPS has an oscillatory pattern with peak-to-peak values up to 100 ns. Analysis of the post fit range residuals shows that for all the examined stations the Galileo residuals exhibit the lowest spread, as small as few decimeters level depending on the multipath, regardless of receiver type and geographical location.

Keywords 1

GNSS constellation, GNSS time scale, Interoperability, GNSS receiver clock

1. Introduction

Interoperability of the GNSSs [1], [2] consists in the use of signals from multiple GNSS constellations to estimate typically the 3D coordinates and velocity of the user. For the Galileo system, the concept of interoperability is made explicit in the Open Service Service Definition Document (OS SDD) Sect. 3.5.1 [3]: *'...One of the main drivers of the Galileo system design has been its interoperability with other GNSS. In the GNSS context, interoperability should be understood as the capability for user equipment to exploit available navigation signals of different GNSS and to produce a combined solution that generally exhibits performance benefits (e.g. better accuracy, higher availability) with respect to the standalone system solution.'*

Specific GNSS - dependent parameters which need to be simultaneously estimated are the receiver clock and clock drift relative to the time scales kept by each GNSS [4]. Receiver clock bias and clock drift are required for appropriate calibration of pseudorange and pseudoDoppler data. The availability of some tens of satellites simultaneously in view makes possible to estimate an additional parameter, a zenith delay. If the ionospheric delay has been removed by using a iono free linear combination of data on two frequencies, then the estimated zenith delay accounts for the tropospheric delay. If single frequency data are used and they are corrected for the ionospheric delay by applying the Klobuchar [5] or NeQuick-G [6] models, then the estimated zenith delay lumps together the residual ionospheric error and the tropospheric delay. Estimating a zenith delay is normally beneficial to improve the stability of the height estimates, provided there is a sufficiently large number of satellites in view.

Navigation with multiple GNSSs thus requires that at each epoch one estimates three coordinates, three velocities, one zenith delay, and as many receiver clocks and clock drifts as the number of tracked

ICL-GNSS 2021 WiP Proceedings, June 01–03, 2021, Tampere, Finland
EMAIL: alessandro.caporali@unipd.it (A. 1); jzurutuza@gmail.com (A. 2)
ORCID: 0000-0002-9831-3907 (A. 1); 0000-0003-3985-5121 (A. 2)

GNSS constellations. Every constellation keeps in fact a time scale non necessarily aligned with that of the other GNSSs to the required accuracy (1 nanosecond (ns) or better). Consequently, the user must synchronize the receiver clock in bias and drift to all the available constellations.

The available data with geodetic quality commercial receivers are at this time the pseudoranges and Doppler in single or dual frequency from GPS [7], Glonass [8], Galileo [3], BeiDou [9], QZSS [10] and NAVIC [11]. Depending on the geographical location, satellites in geostationary orbit (GEO) or inclined geostationary orbits (IGSO) can be used as part of a SBAS (Satellite Based Augmentation System). Examples are the Indian GAGAN or the Japanese MSAS, which provide usable data mostly to users in the Asian regions.

Going deeper into the details of the analysis, the data of the different constellations show remarkable differences. The constants (Earth semimajor axis, flattening, product of the Gravity constant by the Earth's mass) involved in the navigation message are not necessarily identical for the various GNSSs. The algorithm for computation of the satellite ECEF (Earth Centered Earth Fixed) coordinates can be based on the numerical integration of the equations of motion based on an initial vector of state, which is broadcast at intervals typically of 30 minutes (Glonass, SBAS); or on parameters of the osculating Keplerian ellipse plus secular and periodic perturbations of the orbital elements (GPS, Galileo, BeiDou, QZSS, NAVIC), which have different validity times, like, for example, 2 hours for GPS, 4 hours (Galileo), or 30 minutes for GLONASS . Galileo broadcasts two types of navigation messages, I-NAV and F-NAV, to be used depending on the selected L2 frequency used for iono free combination. For Galileo the typical refresh rate of the navigation data broadcast by the satellites ranges from 10 minutes to 3 hours, in order to provide a continuously updated satellite clock model [3].

In this paper we report on a systematic, volume analysis of the coordinates of 19 multiGNSS worldwide sites belonging to the GRC – MS (Galileo Reference Centre – Member States) Reference network using a variety of commercial receiver brands. The GRC-MS is a project coordinated by the GSA (European GNSS Agency) aiming at an independent monitoring of the Galileo Open Service and Commercial Services data dissemination performance. The Principal Investigator is CNES in Toulouse. Our team at the University of Padova is responsible for the monitoring of the interoperability of Galileo with the other GNSSs. The used sites are shown in Fig. 1 (the different colors refer to the different receiver brands) and the equipment is described in Table 1. The worldwide distribution of the GRC-MS multiGNSS sites enables several GNSSs to be tracked. Besides GPS, Glonass, Galileo, BeiDou QZSS and NAVIC/Irnss, we include in our analysis also data from regional Satellite Based Augmentation Systems (SBAS), such as India's GAGAN and Japan's MSAS. Our approach to interoperability spans orbital configurations from Medium Earth Orbit to Geostationary Orbit and Inclined Geosynchronous Orbit.

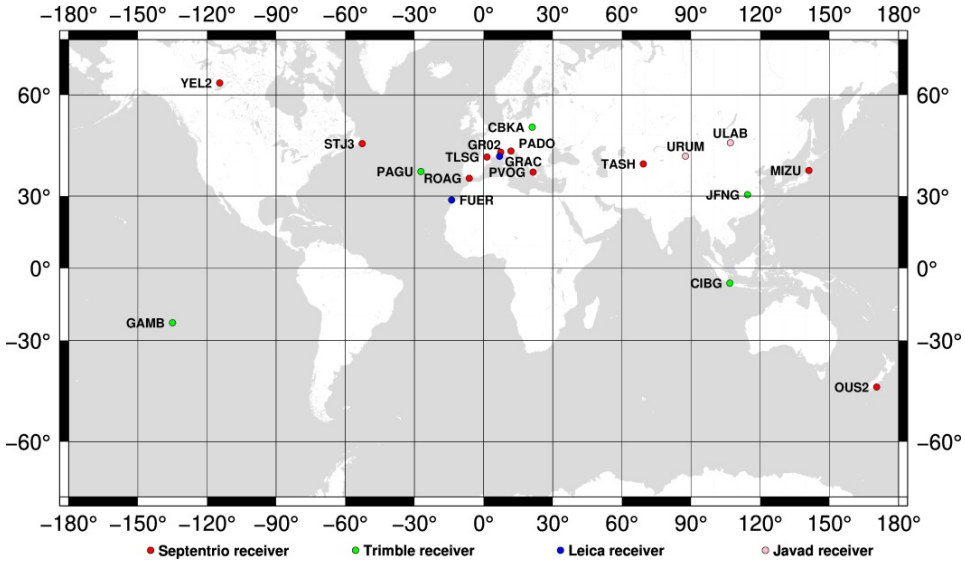

Fig. 1. multiGNSS sites of the GRC network for the interoperability analysis.

2. MultiGNSS software architecture

The software used to carry out all the analysis by UPAD is the in-house developed multiGNSS [12]. The input files are standard RINEX files (observations and navigation files preferably in RINEX v3.04 [13] format, though v2.11 is also admitted); other formats, such as SP3 [14], can be used as well. MultiGNSS is a GNSS analysis software capable of analyzing all the current GNSS constellations: GPS, Glonass, Galileo, Beidou, QZSS, SBAS and NAVIC (former IRNSS). In the preprocessing phase broadcast ephemeris are converted to SP3 format and compared, on a satellite by satellite basis, with a corresponding SP3 precise ephemeris file downloaded from the IGS [15] - MGEX [16] server. The comparison results in 7 Helmert parameters describing the misalignment in origin, orientation and scale of the specific satellite broadcast orbit and clock relative to the corresponding SP3 precise orbit and clock. The results are averaged over all the satellites of the given constellation for the given day, resulting in an average estimate of the 'broadcast reference frame' to the precise reference frame of the SP3 data, which is unique to all the GNSS constellations. In a subsequent processing phase, multiGNSS allows the estimation at each epoch of the three receiver coordinates (ECEF and geodetic with North, East, and Up –NEU- differences relative to a nominal location), one Tropospheric Zenith Delay and nGNSS receiver time offsets, where nGNSS is the number of tracked GNSS constellations. The latter unknowns are the sums of the receiver clock offset and the offset of the GNSS time scale relative to a common time scale. In the post processing phase, differentiation of such an offset relative to the GPS data yields, epoch-wise and for each receiver, estimates of the GNSS time offset to GPS. Comparing across different receivers shows that such offsets can be biased relative to each other by as much as several tens of nanoseconds (ns). Fig. 2 shows the flowchart diagram of multiGNSS.

Table 1
multiGNSS sites of the GRC network for the interoperability analysis (initial equipment).

Agency	Country – Station Location	ID	Receiver Type	AntennaType /Dome
CNES	Canada	STJ3	SEPT POLARX4TR	LEIAR25.R4 NONE
	Canada	YEL2	SEPT POLARX4TR	LEIAR25.R4 NONE
	China	JFNG	TRIMBLE NETR9	TRM59800.00 NONE
	France	TLSG	SEPT POLARX4TR	TRM59800.00 NONE
	French Polynesia	GAMB	TRIMBLE NETR9	TRM59800.00 NONE
	Indonesia	CIBG	LEICA GR10	LEIAR25.R4 NONE
CNIG	Spain	FUER	LEICA GR25	LEIAR20 LEIM
IGN	France	GRAC	LEICA GR25	TRM57971.00 NONE
GFZ	China	URUM	JAVAD TRE_G3TH DELTA	JAV_RINGANT_G5T NONE
	Japan	MIZU	JAVAD TRE_G3TH DELTA	JAV_RINGANT_G3T NONE
	Mongolia	ULAB	JAVAD TRE_G3TH DELTA	JAV_RINGANT_G3T NONE
	New Zealand	OUS2	JAVAD TRE_G3TH DELTA	JAV_RINGANT_G3T NONE
	Uzbekistan	TASH	JAVAD TRE_G3TH DELTA	JAV_RINGANT_G3T NONE
GOP	Greece	PVOG	LEICA GR10	LEIAR10 NONE
INRIM	Italy	GR02	SEPT POLARX4TR	SEPCHOKE_B3E6
ROA	Spain	ROAG	SEPT POLARX4TR	LEIAR25.R4 NONE
SRC	Poland	CBKA	TRIMBLE NETR9	TRM57971.00 NONE
UBI	Azores, Portugal	PAGU	TRIMBLE NETR9	TRM55971.00 NONE
UPAD	Italy	PADO	SEPT POLARX5	SEPTCHOKE_B3E6 SPKE

Several codes are available in the carriers at several frequencies, for the different GNSS constellations. It is not the purpose of this paper to provide an extensive analysis with all the possible combinations of codes modulated on the carriers. Table 2 summarizes the types of signals found in the

RINEX data, coded according to the latest RINEX conventions ([13]: see "Data sources"; RNX 3.05 is already available, but not all the receivers provided observations in this format when this paper is being written). Dual frequency code/phase combinations are generated in order to remove first order ionospheric delays.

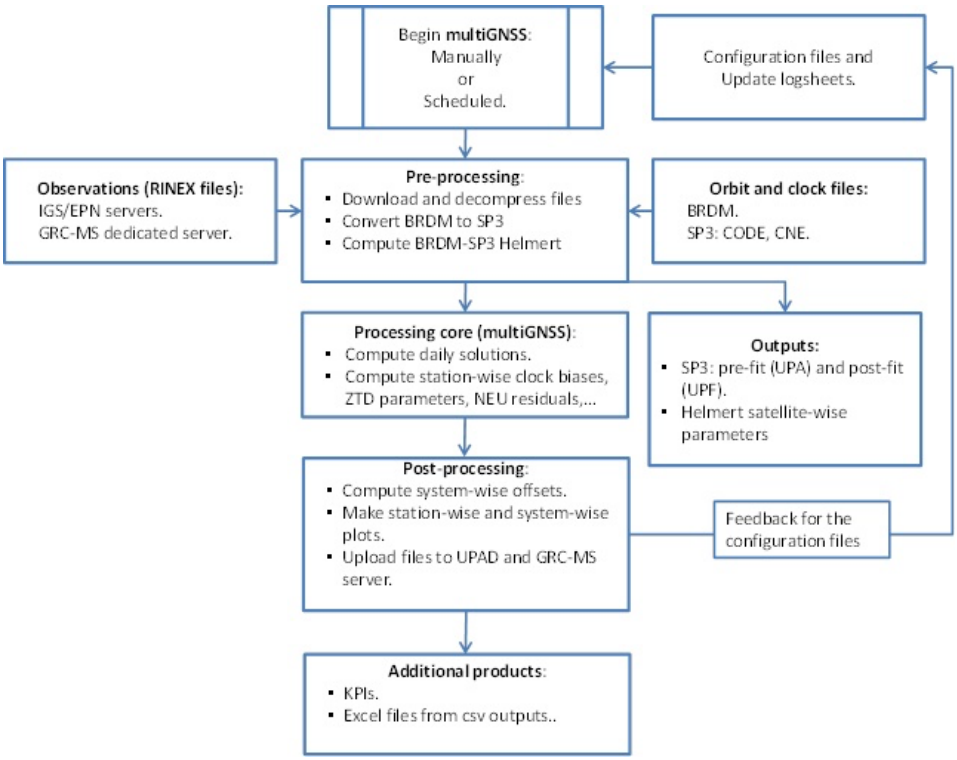

Fig. 2. multiGNSS software flowchart.

Table 2.
Frequency and codes available in the RINEX data for different GNSSs.

System	Carriers/Frequency [MHz]		Coding in RNX 3.04		
GPS	L1 (1575.42)	L2 (1227.60)	C1C	C2W	
Glonass	G1: (1602+k*9/16)	G2: (1246 + k*7/16)	C1C	C2P	
Galileo	E1 (1575.42)	E5b (1207.14)	C1	C7I/C7Q/C7X	I/NAV
	E1 (1575.42)	E5a (1176.45)	C1	C5I/C5Q/C5X	F/NAV
	E1 (1575.42)	E5: E5a+E5b (1191.795)	C1	C8I/C8Q/C8X	I/NAV
BeiDou	B1 (1561.098)	B3 (1268.52)	C1I	C6I/C6Q/C6X	
	B1 (1561.098)	B2b (1207.14)	C1I	C7I/C7Q/C7X	
QZSS	L1 (1575.42)	L2 (1227.60)	C1C	C2S/C2L/C2X	
NAVIC (former IRNSS)	L5 (1176.45)	S (2492.028)	C5A	C9A/C9B/C9C	
GAGAN: SBAS PRNs 127, 128, 132	L1 (1575.42)	L5 (1176.45)	C1C	C5I	
MSAS SBAS PRNs 129, 137	L1 (1575.42)	L5 (1176.45) (not yet)	C1C		

As to SBAS (Satellite-based Augmentation Systems), we use Japan's Multi-functional Satellite Augmentation System (MSAS) and India's GPS and GEO Augmented Navigation (GAGAN). GAGAN

(the Indian SBAS regional system, with satellites with PRN numbers 127, 128 and 132) is at this time the only system delivering valid broadcast messages and pseudoranges in dual frequency. MSAS (the Japanese Satellite Augmentation System, with satellites with PRN numbers 129 and 137) broadcasts navigation messages and single frequency C1 data.

The model of the pseudorange *p(t)* is described in Eq. 1 - 3. Table 3 contains the explanation of the variables.

$$p^i(t) = range^i + c \cdot dt^i(t') + c \cdot (TSC_X + dT_{REC}) + \frac{TZD}{\sin(El^i)} + DCB^i, \text{being,} \quad (1)$$

$$range^i = \quad (2)$$

$$\sqrt{[X^i(t') + \omega_e \cdot Y^i(t-t') - x]^2 + [Y^i(t') - \omega_e \cdot X^i(t-t') - y]^2 + [Z^i(t') - z]^2}($$

$$dt^i(t') = a_0 + a_1 \cdot (t' - T_{oc}) + a_2 \cdot (t' - T_{oc})^2 - \frac{2\sqrt{\mu a}}{c^2} e \cdot \sin\big(E(t')\big) + LS \quad (3)$$

For PVT (Position Velocity and Timing) analysis, pseudoDoppler data are processed simultaneously with the pseudorange data:

$$D^i = -f \frac{\left(\vec{V}^i - \vec{v}\right) \cdot \overrightarrow{los}^i}{c} + f\dot{dT} \quad (4)$$

Where *f* is the carrier frequency, $\vec{V}^i$ and $\vec{v}$ are respectively the ECEF velocity of the *i*-th spacecraft and the receiver, and $\overrightarrow{los}^i$ are the direction cosines. The term ($\dot{dT}$) is the receiver clock drift relative to the given GNSS (independent clock bias and drift are estimated for each constellation). The partial derivative matrix for position and velocity has the same elements, i.e. the direction cosines. The partial derivative for the Tropospheric Zenith Delay (*TZD*) is a 1/cos(*z*) function, *z* being the zenith angle of the satellite.

Table 3.
Explanation of symbols and variables used in Eq.s 1-3.

Symbol	Meaning
$range^i$	Geometric range between satellite i and receiver
c	Speed of light
dt^i	Satellite clock error plus leap seconds (LS), see Eq. 3
T_{oc}	Time of Clock: reference epoch for the polynomial clock model in the first subframe of the navigation message
t'	Time of transmission (satellite clock), corrected from the clock drifts
T	Time of reception (receiver clock)
TSC_X	Time System Correction of the X GNSS System (G = GPS; R = GLONASS; E = Galileo; C = Beidou; M = MSAS; J = QZSS; I = NAVIC; N = GAGAN)
dT_{REC}	Receiver Clock Error
TZD	Tropospheric Zenith Delay
El^i	Elevation of satellite i
DCB^i	Differential Code Bias of satellite I
X^i, Y^i, Z^i	Earth-Centered Earth-Fixed (ECEF) coordinates of satellite i
ω_e	Earth rotation rate (nominal values are defined in the ICD of the various GNSSs)
x, y, z	ECEF coordinates of receiver
a_0, a_1, a_2	Coefficients of broadcast time polynomial satellite time -> system time
μ, a	Gravitational constant times the mass of the earth; major semiaxis of the orbit
$E(t)$	Eccentric anomaly

The vector of the unknowns consists, at each epoch, of three station coordinates, three velocities, one *TZD* and as many ($TSC_X + dT_{REC}$) and their time derivatives as the number of GNSSs constellations

in the analysis. These variables are the sum of a first term dependent on the GNSS but independent of the receiver and a second term independent of the GNSS and dependent on the receiver. To monitor the GNSS specific time bias it is convenient to take TSC_G as reference time scale (subscript $_G$ stands for GPS) and evaluate the difference ($TSC_X + dT_{REC}$) - ($TSC_G + dT_{REC}$), with $_X$ referring to all the GNSSs different from GPS [17], [18], [19]. GPS time was used as reference as it is normally done to broadcast in the navigation message the inter-GNSS time offsets. The following Figures 3 to 9 will show that the measured time offset to GPS time is receiver dependent, and will enable the existence of receiver dependent biases to be investigated for each GNSS, excluding GPS. Table 4 lists these GNSS specific variables, which will be referred to later on.

Table 4.
Definition of the epoch-wise offsets of the GNSS time scales relative to GPS: in the order Glonass, Galileo, BeiDou, QZSS, NAVIC, GAGAN and MSAS.

Time Offset	Definition
GPGA	$(TSC_G+dT_{REC})-(TSC_E+dT_{REC})$
GLGP	$(TSC_R+dT_{REC})-(TSC_G+dT_{REC})$
BDGP	$(TSC_C+dT_{REC})-(TSC_G+dT_{REC})$
QZGP	$(TSC_J+dT_{REC})-(TSC_G+dT_{REC})$
NAGP	$(TSC_I+dT_{REC})-(TSC_G+dT_{REC})$
GNGP	$(TSC_N+dT_{REC})-(TSC_G+dT_{REC})$
MSGP	$(TSC_M+dT_{REC})-(TSC_G+dT_{REC})$

The concept of misalignment of a GNSS specific time scale relative to another (e.g. GPS) is described for Galileo in the OS SDD [3] section 3.5.1.1: *'…Galileo System Time (GST) …. and GPS time are two independent continuous timescales steered respectively to UTC(k) and UTC(USNO)…. hence Galileo and GPS system times are different and this difference is variable with time…*'. Figure 3 shows the difference between GPS time and GST with different receivers at different locations during year 2020. Q1 to Q4 represent the Quarters of the GRC-MS Project (in year_day of the year style, 2020 Q1 starts 20_001; Q2 starts 20_092; Q3 starts 20_183; Q4 starts 20_275). Clearly all the receivers measure the same signal modulo a very nearly constant offset which depends on the receivers themselves. This dependence on the receiver implies that broadcasting a single Galileo to GPS time offset (GGTO [20]) enables only specific, carefully calibrated receivers, to benefit from this information. Other receivers (normally a commercial receiver of geodetic quality) need to synchronize to Galileo and GPS time scales using independent variables.

Figure 3 also shows that the difference between the Galileo and GPS time scales remains normally within +/- 5 nsec, except in rare situations, such as in Q1 (2020/01/29), where the relative offset was reset by ca. 12 nsec. To understand whether the reset is attributable to the GPS or Galileo system times, it is valuable to investigate the offsets to GPS times measured by the same receivers with other GNSSs. The following figures (Figure 4 to 9) describe the Glonass to GPS time offset, the BeiDou to GPS time offset, the QZSS to GPS time offset, the NAVIC to GPS time offset, and eventually the two regional SBAS systems GAGAN and MSAS to GPS time offsets. The conclusion is clearly that the Q1 GPGA event is most probably attributable to a reset in the Galileo system time, because there is no evidence of a 12 ns discontinuity for the other constellations referred to GPS time.

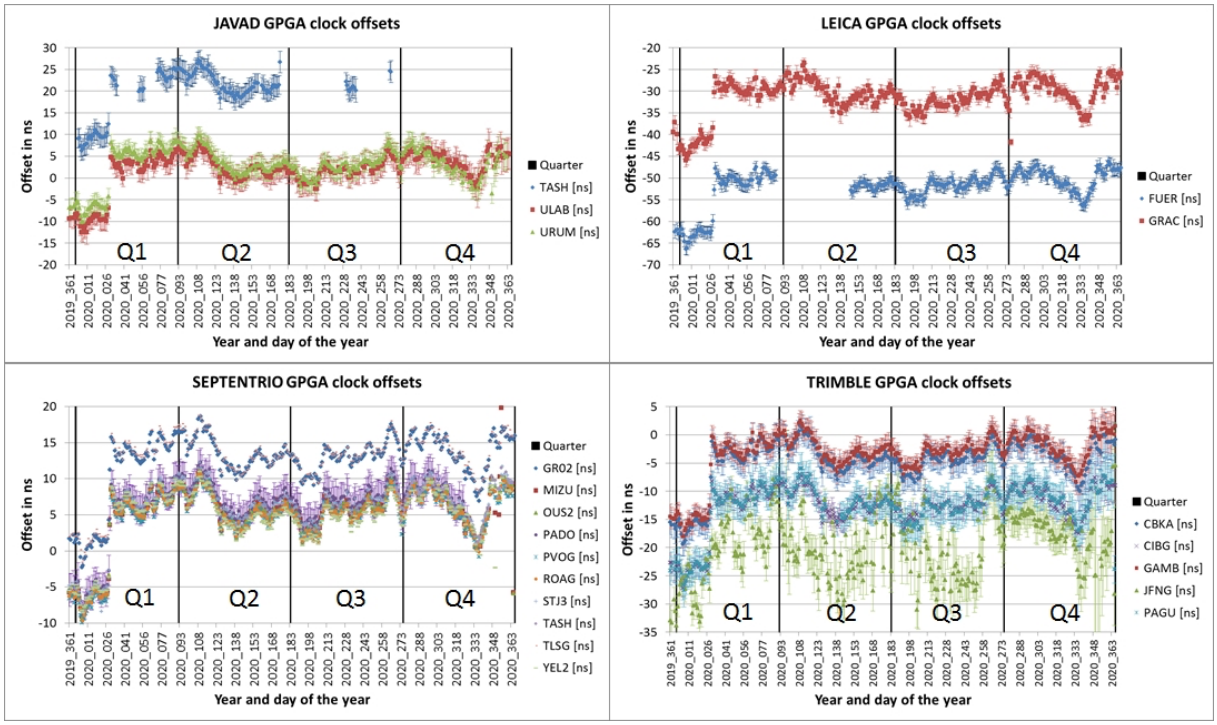

Fig. 3. Temporal changes of the daily GPS to Galileo system time offset measured with different commercial multiGNSS receivers in various locations worldwide during 4 quarters Q1 … Q4 in 2020. The relative offset is caused by receiver dependent biases. Y axis are the offsets in (ns); X axis units are in the form year_day of year.

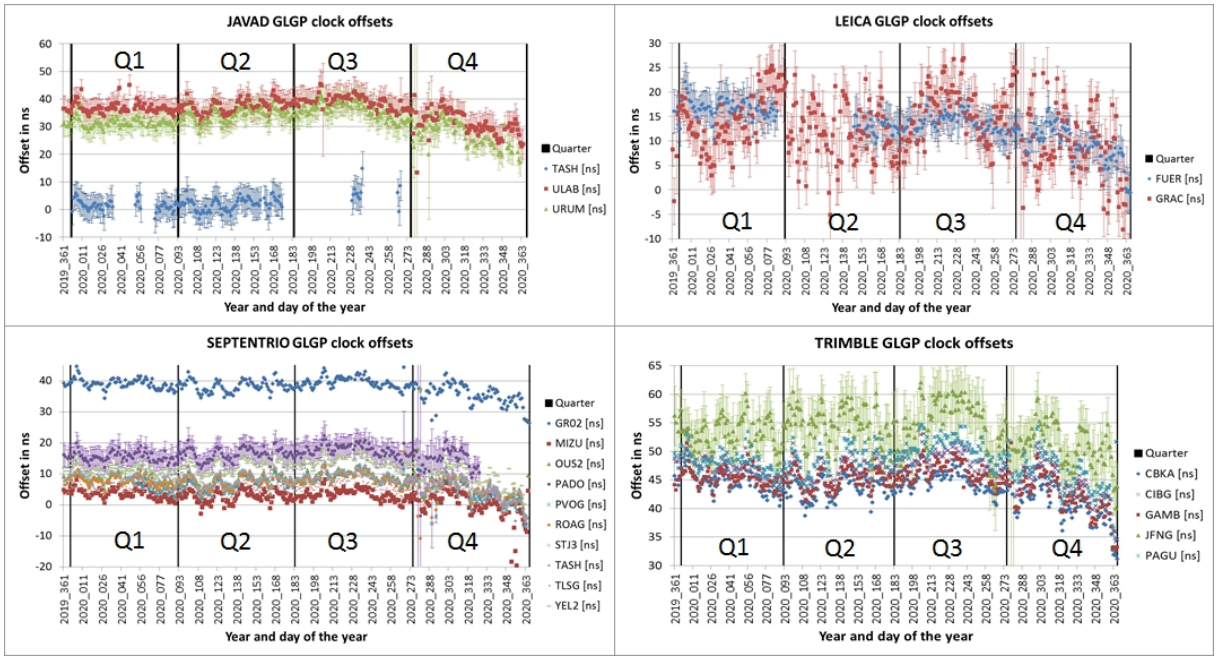

Fig. 4. Daily estimates of the Glonass to GPS time offset measured with different receivers at stations distributed worldwide. Y axis are the offsets in (ns); X axis units are in the form year_day of year.

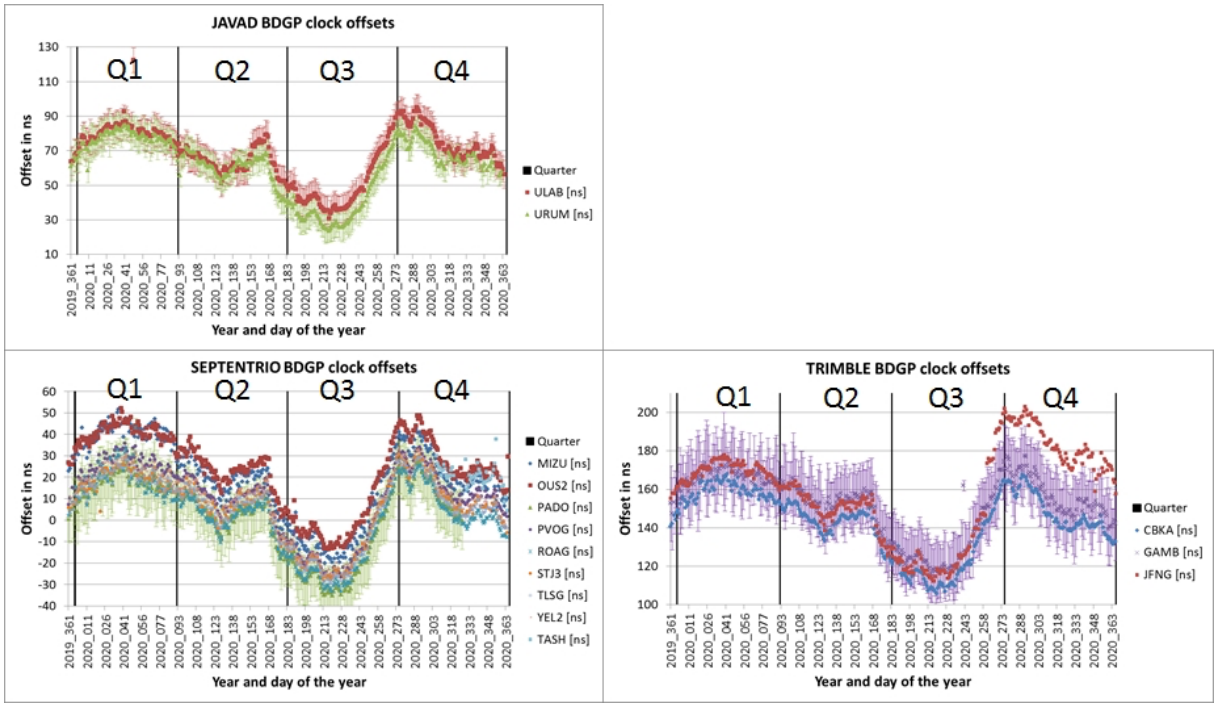

Fig. 5. Daily estimates of the BeiDou to GPS time offset measured with different receivers at stations distributed worldwide. Y axis shows the offsets (ns); X axis units are year_day of year.

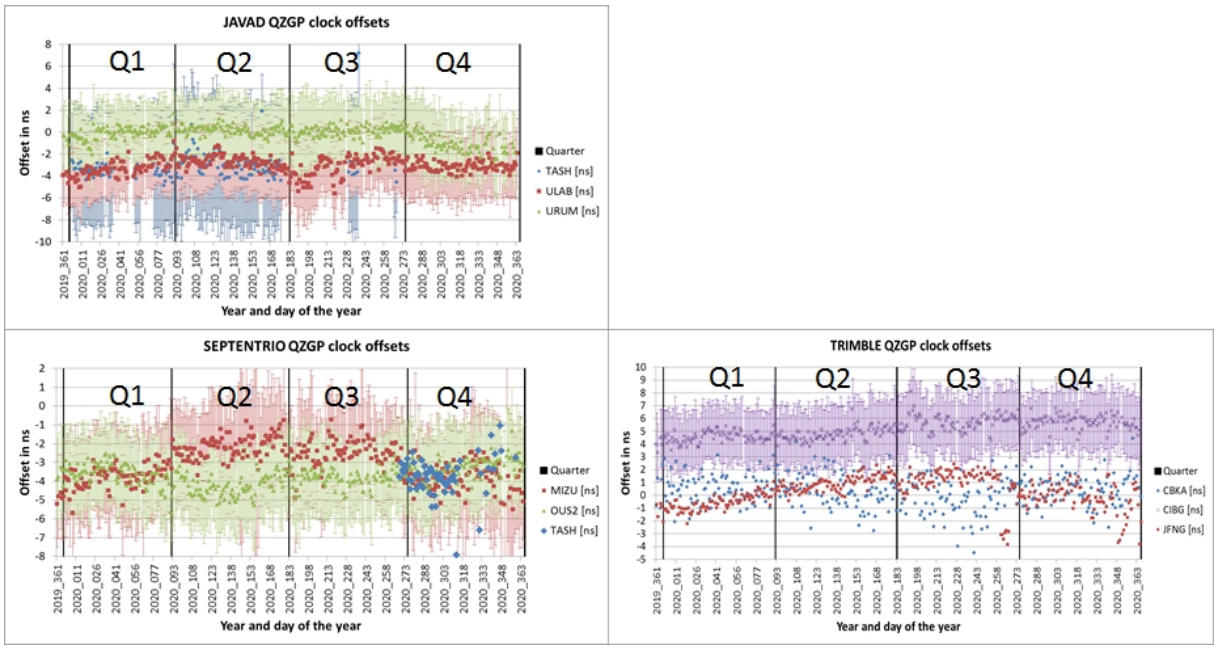

Fig. 6. Daily estimates of the QZSS to GPS time offset measured with different receivers at stations distributed worldwide. Y axis shows the offsets (ns); X axis units are year_day of year.

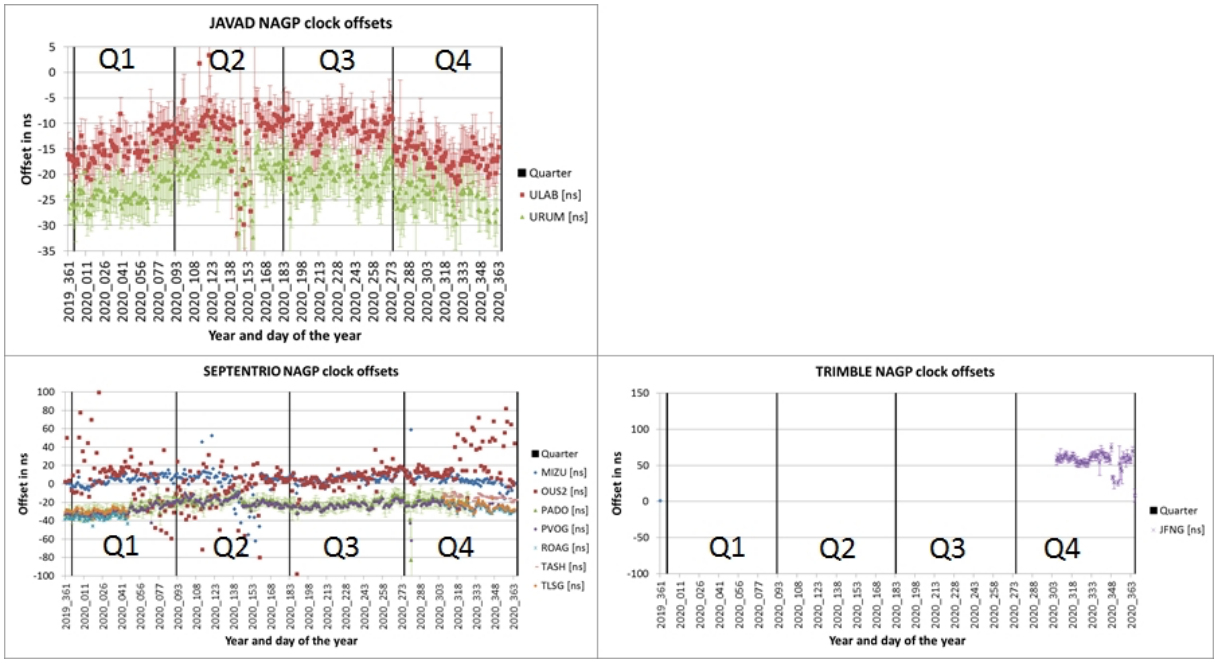

Fig. 7. Daily estimates of the NAVIC to GPS time offset measured with different receivers at stations distributed worldwide. Y axis shows the offsets (ns); X axis units are year_day of year.

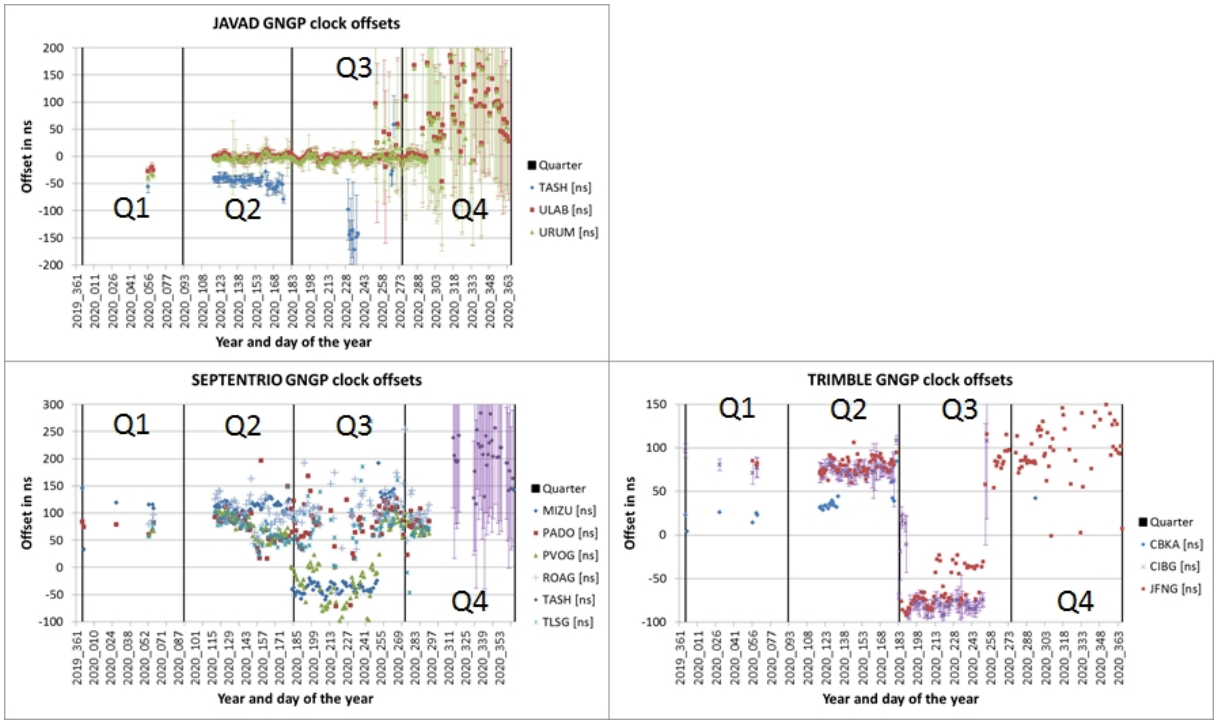

Fig. 8. Daily estimates of the GAGAN to GPS time offset measured with different receivers at stations distributed mostly in the Middle Far East. Y axis shows the offsets (ns); X axis units are year_day of year.

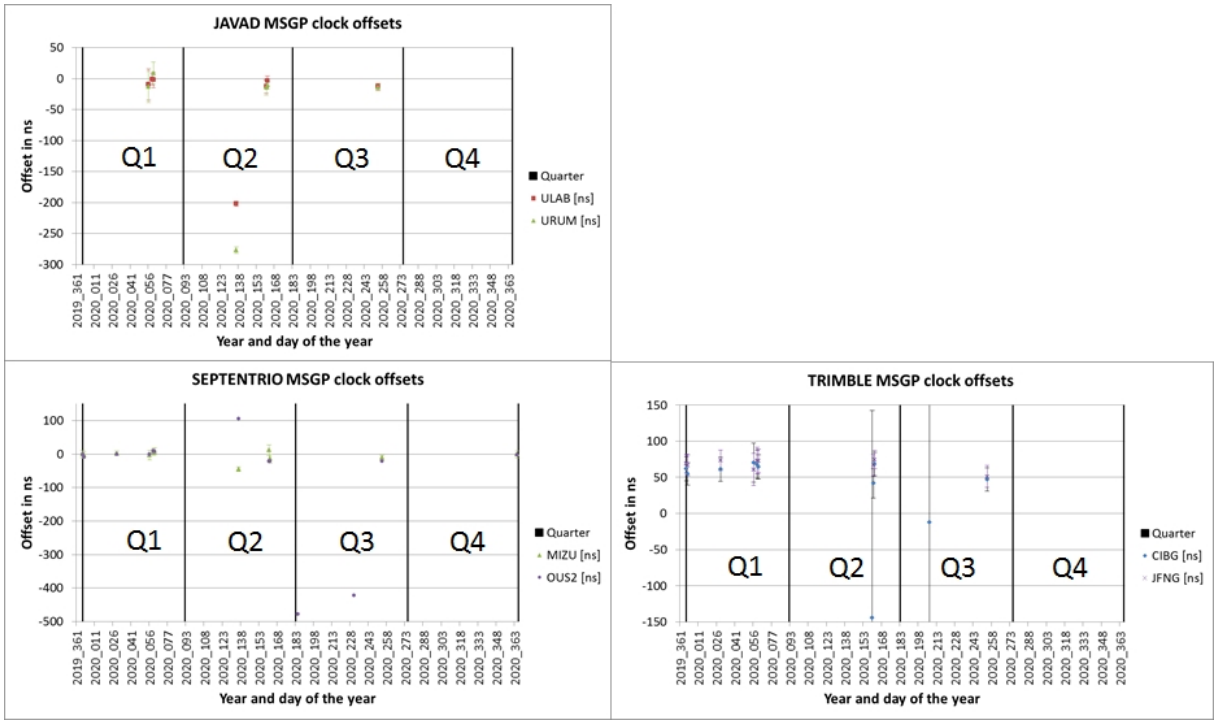

Fig. 9. Daily estimates of the MSAS to GPS time offset measured with different receivers at stations distributed mostly in the Middle Far East. Y axis shows the offsets (ns); X axis units are year_day of year.

3. Comparative GNSS performance in positioning

The GNSS data are used in one daily joint solution. Coordinates, velocities and TZD are parameters in common for all the tracked GNSSs. We compute them at 15 min. intervals, and then evaluate the mean and root mean square (r.m.s.) errors across one day. Table 4 (Q1 And Q2) and Table 5 (Q3 and Q4) summarize sample results at test days in 2020, with separate statistics depending on the GNSS, and on the station/receiver. Here we provide some example results, and the detailed data are available as part of the final documentation of the GRC-MS Project. Table 4 and Table 5 show that in comparison with other GNSSs, Galileo pseudorange residuals have the lowest r.m.s. dispersion, regardless of receiver type, day and geographical location. In particular the station FUER, in the Canary Islands (Spain), has systematically an r.m.s. spread as low as 0.5 m, which is most probably caused by favorable multipath conditions relative to the other receivers. FUER in fact has a comparatively low r.m.s. also with GPS and Glonass.

Table 4.

Daily averaged post-fit residuals of the multiGNSS combined solution for different days for PADO (SEPTENTRIO), URUM (JAVAD), FUER (Leica) and CBKA (TRIMBLE), including Q1 (days 001, 032 and 063) and Q2 solutions (days 093/095, 124 and 156).

				2020_001 (Q1)				
Site	**Rec. Type**	**GPS (m)**	**GLO (m)**	**GAL (m)**	**BDS (m)**	**QZSS (m)**	**IRN (m)**	**GAGAN (m)**
PADO	**SEPTENTRIO**	-0.05±1.52	0.05±2.46	0.00±1.20	2.12±7.60		0.00±1.71	
URUM	**JAVAD**	0.00±1.51	0.00±2.96	0.00±1.04	0.98±7.25	0.00±1.05	0.00±2.30	
FUER	**LEICA**	0.00±1.21	0.00±2.58	0.00±0.59				
CBKA	**TRIMBLE**	0.00±1.75	0.00±2.51	0.00±1.30	0.41±6.79			
				2020_032 (Q1)				
Site	**Rec. Type**	**GPS (m)**	**GLO (m)**	**GAL (m)**	**BDS (m)**	**QZSS (m)**	**IRN (m)**	**GAGAN (m)**
PADO	**SEPTENTRIO**	0.00±1.38	0.00±2.58	0.00±0.97	0.90±7.22		0.00±1.99	
URUM	**JAVAD**	0.00±1.61	0.00±3.15	0.00±1.00	1.02±6.76	0.00±0.92	0.00±2.10	
FUER	**LEICA**	0.00±1.27	0.00±3.01	0.00±0.51				

CBKA	**TRIMBLE**	0.00±1.72	0.00±2.75	0.00±1.17	0.17±6.37			
					2020_063 (Q1)			
Site	**Rec. Type**	**GPS (m)**	**GLO (m)**	**GAL (m)**	**BDS (m)**	**QZSS (m)**	**IRN (m)**	**GAGAN (m)**
PADO	**SEPTENTRIO**	0.00±1.56	0.00±2.27	0.00±1.05	1.50±7.33		0.00±1.61	
URUM	**JAVAD**	0.00±1.66	0.00±3.17	0.00±1.31	1.00±7.10	0.00±1.05	0.00±2.00	
FUER	**LEICA**	0.00±1.32	0.00±2.84	0.00±0.46				
CBKA	**TRIMBLE**	0.00±1.84	0.00±2.58	0.00±1.22	0.55±6.72			
					2020_093 (095 for URUM) (Q2)			
Site	**Rec. Type**	**GPS (m)**	**GLO (m)**	**GAL (m)**	**BDS (m)**	**QZSS (m)**	**IRN (m)**	**GAGAN (m)**
PADO	**SEPTENTRIO**	-0.02±1.65	0.03±2.59	-0.17±1.83	1.45±7.07		0.00±2.57	
URUM	**JAVAD**	0.00±1.43	0.00±2.83	0.00±1.01	0.56±6.34	0.00±0.87	-0.05±2.86	
FUER	**LEICA**	-	-	-				
CBKA	**TRIMBLE**	0.00±1.77	0.00±2.65	0.00±1.18	0.00±6.64			
					2020_124 (Q2)			
Site	**Rec. Type**	**GPS (m)**	**GLO (m)**	**GAL (m)**	**BDS (m)**	**QZSS (m)**	**IRN (m)**	**GAGAN (m)**
PADO	**SEPTENTRIO**	0.00±1.57	0.06±2.51	0.00±1.09	0.95±7.50		0.00±2.5	
URUM	**JAVAD**	0.00±1.40	0.02±3.09	0.00±1.11	0.79±6.61	0.00±0.90	0.00±2.94	
FUER	**LEICA**	-	-	-				
CBKA	**TRIMBLE**	0.00±1.67	0.00±2.54	0.00±1.15	-0.24±6.62			
					2020_156 (Q2)			
Site	**Rec. Type**	**GPS (m)**	**GLO (m)**	**GAL (m)**	**BDS (m)**	**QZSS (m)**	**IRN (m)**	**GAGAN (m)**
PADO	**SEPTENTRIO**	-0.02±1.75	-0.04±2.54	-0.12±1.65	1.67±6.93		0.00±1.94	
URUM	**JAVAD**	0.00±1.42	0.00±3.09	0.00±1.34	0.20±6.64	0.00±0.86	-0.05±4.77	0.00±4.74
FUER	**LEICA**	0.00±1.25	0.00±2.70	0.00±0.50				
CBKA	**TRIMBLE**	0.00±1.70	0.00±2.50	0.00±1.20	-0.06±6.30			

Table 5.

Daily averaged post-fit residuals of the multiGNSS combined solution for different days for PADO (SEPTENTRIO), URUM (JAVAD), FUER (Leica) and CBKA (TRIMBLE), including Q3 solutions (doys 183, 214, 245) and Q4 (doys 275, 306 and 340).

					2020_183 (Q3)			
Site	**Rec. Type**	**GPS (m)**	**GLO (m)**	**GAL (m)**	**BDS (m)**	**QZSS (m)**	**IRN (m)**	**GAGAN (m)**
PADO	**SEPTENTRIO**	0.00±1.61	-0.03±2.38	0.00±1.23	1.60±6.99		0.00±3.02	
URUM	**JAVAD**	0.00±1.45	0.00±3.27	0.00±1.24	0.39±6.41	0.00±1.06	0.00±2.66	0.00±3.93
FUER	**LEICA**	0.00±1.29	0.00±2.94	0.00±0.58				
CBKA	**TRIMBLE**	0.00±1.65	0.00±2.67	0.00±1.15	-0.03±6.50			
					2020_214 (Q3)			
Site	**Rec. Type**	**GPS (m)**	**GLO (m)**	**GAL (m)**	**BDS (m)**	**QZSS (m)**	**IRN (m)**	**GAGAN (m)**
PADO	**SEPTENTRIO**	-0.04±1.53	-0.06±2.89	0.00±1.04	0.68±6.98		0.00±2.73	
URUM	**JAVAD**	0.00±1.41	0.00±2.96	0.00±1.29	0.23±6.63	0.00±0.93	0.00±2.44	0.00±3.01
FUER	**LEICA**	0.00±1.27	0.00±2.61	0.00±0.51				
CBKA	**TRIMBLE**	0.00±1.68	0.00±2.66	0.00±1.16	-0.26±6.15			
					2020_245 (Q3)			
Site	**Rec. Type**	**GPS (m)**	**GLO (m)**	**GAL (m)**	**BDS (m)**	**QZSS (m)**	**IRN (m)**	**GAGAN (m)**
PADO	**SEPTENTRIO**	0.03±1.56	-0.01±2.56	-0.24±1.58	1.67±7.35		0.00±1.86	
URUM	**JAVAD**	0.00±1.48	0.02±3.12	0.00±1.97	0.35±6.32	0.00±0.99	0.00±2.82	
FUER	**LEICA**	0.00±1.23	0.00±2.55	0.00±0.49				
CBKA	**TRIMBLE**	0.00±1.79	0.00±2.40	0.18±1.51	-0.04±6.44			
					2020_275 (Q4)			
Site	**Rec. Type**	**GPS (m)**	**GLO (m)**	**GAL (m)**	**BDS (m)**	**QZSS (m)**	**IRN (m)**	**GAGAN (m)**
PADO	**SEPTENTRIO**	-0.03±2.63	0.06±2.77	0.05±1.32	1.36±7.00		0.00±2.08	
URUM	**JAVAD**	0.00±1.68	0.00±3.26	0.00±1.47	0.35±6.28	0.00±1.00	0.00±2.98	-0.86±9.59
FUER	**LEICA**	0.00±1.32	0.00±3.07	0.00±0.52				

CBKA	**TRIMBLE**	0.00±1.77	0.00±2.63	0.00±1.10	-0.04±6.36			
					2020_306 (Q4)			
Site	**Rec. Type**	**GPS (m)**	**GLO (m)**	**GAL (m)**	**BDS (m)**	**QZSS (m)**	**IRN (m)**	**GAGAN (m)**
PADO	**SEPTENTRIO**	-0.04±1.64	0.03±2.56	0.00±1.31	1.17±6.92		0.00±2.47	
URUM	**JAVAD**	-0.04±1.41	0.00±2.88	0.00±1.15	0.82±6.53	0.00±1.01	0.00±2.08	
FUER	**LEICA**	0.00±1.19	0.00±2.49	0.00±0.48				
CBKA	**TRIMBLE**	0.00±1.64	-0.02±2.39	0.00±1.06	-0.20±6.31			
					2020_340 (Q4)			
Site	**Rec. Type**	**GPS (m)**	**GLO (m)**	**GAL (m)**	**BDS (m)**	**QZSS (m)**	**IRN (m)**	**GAGAN (m)**
PADO	**STONEX**	0.04±1.73	0.74±3.97	-0.04±1.68	1.17±6.87		0.00±1.56	
URUM	**JAVAD**	0.00±1.64	0.02±2.97	-0.36±2.36	0.61±6.52	0.00±1.04	0.00±2.20	
FUER	**LEICA**	0.00±1.41	0.00±2.84	-0.31±1.56				
CBKA	**TRIMBLE**	0.00±1.71	0.00±2.47	-0.48±2.26	-0.40±6.07			

For the sake of completeness, in Table 6, we provide the multiGNSS solutions of two of the days of 2020 that have the largest number of MSAS available solutions. These are days 002 (2020/01/02) and 029 (2020/01/29). The stations are located in western Asia (ULAB is located in Mongolia; URUM is located in China; MIZU is located in Japan; OUS2is located in New Zealand; CIBG is located in Indonesia; JFNG is located in China) where the satellites PRN 129 and PRN 137 are visible and these satellites are also flagged as "HEALTHY" in the broadcast navigation message. In view of the few MSAS available solutions we can say that, according to the r. m. s of the daily post-fit residuals, MSAS performs worse than QZSS, but similar to NAVIC and better than its Indian counterpart GAGAN.

Table 6.
Daily averaged post-fit residuals of the multiGNSS combined solution, including MSAS, for different days for ULAB and URUM (JAVAD); MIZU and OUS2 (SEPTENTRIO), and CIBG and JFNG (TRIMBLE), solutions (days of the 2020 year 002 and 029, which correspond with 2020/01/02 and 2020/01/29 respectively).

					2020_002				
Site	**Rec. Type**	**GPS (m)**	**GLO (m)**	**GAL (m)**	**BDS (m)**	**QZSS (m)**	**IRN (m)**	**GAGAN (m)**	**MSAS (m)**
ULAB	**JAVAD**	0.00±1.62	0.00±3.29	0.00±1.34	0.86±6.99	0.00±1.05	0.00±1.63		
URUM	**JAVAD**	0.00±1.78	0.00±3.19	0.00±1.05	0.62±7.11	0.00±0.95	0.00±2.12		
MIZU	**SEPTENTRIO**	0.00±1.41	0.00±2.16	0.00±0.83	0.53±6.80	0.00±0.62	0.00±1.87		0.00±2.28
OUS2	**SEPTENTRIO**	0.00±1.52	0.00±2.48	0.00±0.98	1.50±7.58	0.00±0.75			0.00±2.44
CIBG	**TRIMBLE**	0.00±1.42	0.00±2.78	0.00±0.86		0.00±0.97			0.00±3.39
JFNG	**TRIMBLE**	0.00±1.63	0.00±2.76	0.00±0.95	0.14±6.60	0.00±0.91			0.00±3.71
					2020_029				
Site	**Rec. Type**	**GPS (m)**	**GLO (m)**	**GAL (m)**	**BDS (m)**	**QZSS (m)**	**IRN (m)**	**GAGAN (m)**	**MSAS (m)**
ULAB	**JAVAD**	0.00±1.61	-0.03±3.37	0.00±1.46	0.86±7.11	0.00±1.25	0.00±1.82		0.00±1.34
URUM	**JAVAD**	0.00±1.44	0.00±2.86	0.00±0.89	0.44±7.03	0.00±0.92	0.00±1.84	0.00±3.12	
MIZU	**SEPTENTRIO**	0.00±1.36	0.00±1.83	0.00±0.75	0.19±6.58	0.00±0.71	0.00±2.64		0.00±1.18
OUS2	**SEPTENTRIO**	0.00±1.45	0.00±2.04	0.00±0.85	1.98±7.57	0.00±0.81			0.00±1.17
CIBG	**TRIMBLE**	0.00±1.48	0.00±2.35	0.00±0.85		0.00±0.97			
JFNG	**TRIMBLE**	0.00±1.58	0.00±2.32	0.00±1.05	0.22±6.55	0.00±0.93			0.00±3.03

4. Conclusions

Positioning and Navigation already at present uses data from multiple constellations. Hence the need for an accurate intercalibration of the data coming from different sources. We have shown that the alignment of the receiver clock to different time scales, one for each tracked GNSS is varying in time, is receiver dependent and cannot be predicted with sufficient accuracy. Therefore the need to estimate

a clock bias for every constellation for each epoch. The receiver synchronization to the various GNSS time scales is done simultaneously with the estimate of the receiver coordinates. Our results are based on iono free pseudoranges and broadcast ephemeris. The inference is that Galileo pseudorange residuals are the lowest for all epochs and receiver types in 2020. The r.m.s. of Galileo residuals ranges for 0.5 m to 1.5 m depending on receiver and location, with broadcast ephemeris. These figures can certainly be lowered with ephemeris of higher quality such as those in the SP3 data files of the MGEX project.

5. Acknowledgements

We acknowledge the European Union and the European GNSS Agency (GSA) for supporting the cooperation of the Galileo Reference Center (GRC) [21] with Member States within the GRC-MS project, and co-financed (Grant agreement nr. GSA/GRANT/04/2016), in support of an independent monitoring of the Galileo system performance.

6. References

[1] Januszewski J.: Compatibility and Interoperability of Satellite Navigation Systems, 11th International Conference "Computer Systems Aided Science, Industry and Transport", Transcomp 2007, vol.1, 289-294 (2007).

[2] Stansell, T.A., Jr.: GNSS Interoperability. In Position, Navigation, and Timing Technologies in the 21st Century (eds Y.T.J. Morton, F. Diggelen, J.J. Spilker, B.W. Parkinson, S. Lo and G. Gao). https://doi.org/10.1002/9781119458449.ch9 (2020).

[3] Galileo Open Service - Service Definition Document (OS SDD v1.1), https://www.gsc-europa.eu/sites/default/files/sites/all/files/Galileo-OS-SDD_v1.1.pdf, last accessed 2021/04/05.

[4] Januszewski J.: Time, its scales and part in satellite navigation systems. Scientific Journals Maritime University of Szczecin, No.20(92), 52−59 (2010).

[5] Klobuchar, J.: Ionospheric Time-Delay Algorithms for Single-Frequency GPS Users. IEEE Transactions on Aerospace and Electronic Systems (3), pp. 325-331 (1987).

[6] European Union. European GNSS (Galileo) Open Service-Ionospheric Correction Algorithm for Galileo Single Frequency Users. 1.2, https://www.gsc-europa.eu/sites/default/files/sites/all/files/Galileo_Ionospheric_Model.pdf, last accessed 2021/04/05.

[7] GPS Interface Control Document ICD-GPS-870, https://www.gps.gov/technical/icwg/ICD-GPS-870C.pdf, last accessed 2021/04/05

[8] GLONASS INTERFACE CONTROL DOCUMENT, http://russianspacesystems.ru/wp-content/uploads/2016/08/ICD-GLONASS-CDMA-General.-Edition-1.0-2016.pdf, last accessed 2021/04/05.

[9] BeiDou Navigation Satellite System Signal In Space Interface Control Document Open Service Signal (Version 2.1), http://en.beidou.gov.cn/SYSTEMS/ICD/201806/P020180608523308843290.pdf, last accessed 2021/04/05.

[10] Quasi-Zenith Satellite System Interface Specification Satellite Positioning, Navigation and Timing Service (IS-QZSS-PNT-004), https://qzss.go.jp/en/technical/download/pdf/ps-is-qzss/is-qzss-pnt-004.pdf?t=1617735261287, last accessed 2021/04/05.

[11] Indian Regional Navigation Satellite System, https://www.isro.gov.in/sites/default/files/irnss_sps_icd_version1.1-2017.pdf, last accessed 2021/04/05.

[12] Nicolini, L. and Caporali, A. Investigation on Reference Frames and Time Systems in Multi-GNSS. Remote Sensing. (2018), 10(1), 80; https://doi.org/10.3390/rs10010080

[13] RINEX: The Receiver Independent Exchange Format Version 3.04, https://files.igs.org/pub/data/format/rinex304.pdf, last accessed 2021/04/05.

[14] Hilla, S. The Extended Standard Product 3 Orbit Format (SP3-d) https://gssc.esa.int/wp-content/uploads/2018/07/sp3d.pdfftp://igs.org/pub/data/format/sp3d.pdf, last accessed 2021/04/05.

[15] Johnston, G., Riddell, A., Hausler, G. The International GNSS Service. Teunissen, Peter J.G., & Montenbruck, O. (Eds.), Springer Handbook of Global Navigation Satellite Systems (1st ed., pp. 967-982). Cham, Switzerland (2018). Springer International Publishing. DOI: 10.1007/978-3-319-42928-1.
[16] Montenbruck, O.; Steigenberger, P.; Hauschild, A. Broadcast versus precise ephemerides: A multi-GNSS perspective. GPS Solut. 2015, 19, 321–333.
[17] Odijk, D.; Teunissen, P.J.G. Characterization of between-receiver GPS-Galileo inter-system biases and their effect on mixed ambiguity resolution. GPS Solut. (2013), 17, 521–533.
[18] Jiang, N.; Xu, Y.; Xu, T.; Xu, G.; Sun, Z.; Schuh, H. GPS/BDS short-term ISB modelling and prediction. GPS Solut. (2017), 21, 163–175.
[19] Chen J, Wang J, Zhang Y, Yang S, Chen Q, Gong X. Modeling and assessment of GPS/BDS combined precise point positioning. Sensors (2016) 16(7):1151. doi:10.3390/s16071151.
[20] Vanschoenbeek, I., Bonhoure, B., Boschetti, M. and Legenne, J. GNSS Time Offset Effect on GPS-Galileo Interoperability Performance. InsideGNSS, pp. 60–70, September/October, 2007.
[21] Buist, P.; Mozo, A.; Tork, H. Overview of the Galileo Reference Centre: Mission, Architecture and Operational Concept. Proceedings of the 30th International Technical Meeting of the Satellite Division of The Institute of Navigation (ION GNSS+ 2017); , 2017; pp. 1485–1495. doi:10.33012/2017.15371